Meson exchange currents in the ^{3}He$(\gamma,\pi^+)^3$H reaction

J. A. Gómez Tejedor, S. S. Kamalov,* and E. Oset
Departamento de Física Teórica and Instituto de Física Corpuscular,
Centro Mixto Universidad de Valencia–Consejo Superior de Investigaciones Científicas, 46100 Burjassot (Valencia), Spain
(Received 18 June 1996)

We generate meson exchange currents mechanisms for the (γ,π^+) reaction in nuclei starting from the $\gamma N\to\pi\pi N$ amplitude on one nucleon and allowing one of the pions to be produced off shell and be absorbed by a second nucleon. Detailed calculations are presented for the $\gamma\ ^3\mathrm{He}\to\pi^+{}^3\mathrm{H}$ reaction, where we show that the cross section at large momentum transfers is dominated by these mechanisms, helping improve the agreement with experimental data. It is also shown that the meson exchange currents produce important effects in the photon asymmetry in the Δ-resonance region. [S0556-2813(96)04512-8]

PACS number(s): 25.20.Lj, 21.30.Cb, 24.10.Eq, 25.10.+s

I. INTRODUCTION

Conventional calculations using the impulse approximation and multiple scattering, together with Faddeev wave functions, have succeeded in reproducing the data of pion scattering and photoproduction on the trinucleon system up to about $Q^2<6$ fm^{-2} [1–3].

However, at larger momentum transfers present calculations fail to reproduce the data of the ^{3}He$(\gamma,\pi^+)^3$H reaction [1] and similar problems show up in coherent π^0 photoproduction [4] or pion elastic scattering [5].

Some steps to generate meson exchange currents (MEC's) in pion photoproduction in nuclei were given in Ref. [6], imposing current conservation and gauge invariance as leading principles and making an expansion in powers of $1/M$ (M is the nucleon mass).

A different approach, which was also based on the gauge invariance of the nuclear pion photoproduction amplitude, is taken in Ref. [7] with apparent improvements on the region of high momentum transfers in the ^{3}He$(\gamma,\pi^+)^3$H reaction. A critical discussion of this approach will be made in the next section.

In the present paper we shall follow a different approach: By analogy with the way the two-body photon absorption is generated from the $\gamma N\to\pi N$ amplitude [8–10], we shall construct two-body currents for the (γ,π^+) reaction in nuclei starting from the $\gamma N\to\pi\pi N$ amplitude, which is the object of recent experimental [11,12] and theoretical [13–15] study. As we shall see, the effects obtained at large momentum transfers are sizable but some indeterminations remain, tied to the precise value of the $\Delta\Delta\pi$ and $\Delta\Delta\rho$ couplings for which the present reaction sets some upper bounds.

II. TWO-BODY EXCHANGE CURRENTS FOR THE (γ,π) REACTION

The mechanisms for two-body photon absorption used in [8–10] are generated in the following way. One starts from the $\gamma N\to\pi N$ amplitude as depicted diagrammatically in Fig. 1(a). If the pion is produced with an off-shell kinematics, it can be absorbed by one of the other nucleons in the nucleus and we generate in this way two-nucleon absorption mechanisms, as shown in Fig. 1(b).

For the nuclear (γ,π) reaction the procedure is analogous. We start now with a model for the $\gamma N\to\pi\pi N$ reaction, as depicted in Fig. 2(a), and then produce one of the pions off shell and let it be absorbed by a second nucleon, as depicted in Fig. 2(b).

The model of Ref. [13] uses 67 Feynman diagrams to treat the $\gamma p\to\pi^+\pi^- p$ reaction. The model considers the coupling of photons to nucleons and resonances and the coupling of these resonances to pions and nucleons or other resonances. The model includes $N,\Delta(1230)$, $N^*(1440)$, and $N^*(1520)$ resonances. The model of Ref. [15] is much more simplified but includes some unitary corrections which are only relevant at photon energies above 800 MeV, beyond the scope of the present work. Here we follow the version of the model described in [14] which keeps only the 20 Feynman diagrams which are needed for energies below 800 MeV. On the other hand, in Ref. [14] the model of Ref. [13] is extended to account for the different isospin channels, which need to be considered here.

Before proceeding forward let us make some comments about the two-body mechanisms considered in Ref. [7]. Diagrammatically they are depicted in Fig. 3 and they are evaluated using time-dependent perturbation theory, taking ^{3}He or ^{3}H wave functions for the initial and final states and sum-

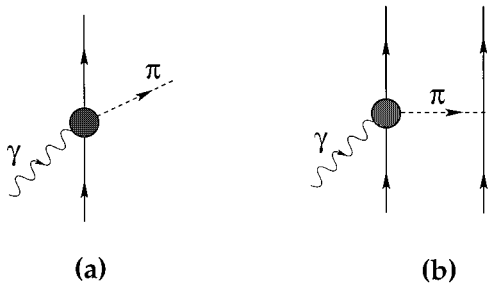

FIG. 1. (a) Feynman diagram for pion photoproduction on the nucleon, (b) meson exchange current mechanism associated with diagram (a).

*Permanent address: Laboratory of Theoretical Physics, JINR Dubna, Head Post Office Box 79, SU-101000 Moscow, Russia.

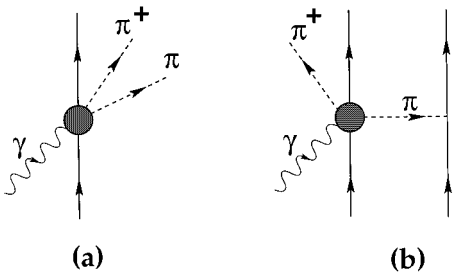

FIG. 2. (a) Feynman diagrams for two-pion photoproduction on the nucleon; (b) meson exchange current mechanism associated with diagram (a).

ming over a set of intermediate states which contain only three nucleons, for which plane waves are assumed.

On the other hand, an alternative, time-independent Feynman diagrammatic perturbation approach would manifestly exchange mesons between the nucleons, as shown in Fig. 4, which would transfer the photon energy from one nucleon to the other. In the case of one-pion exchange, the pion propagator can become singular, corresponding to on-shell pion production, in which case, this contribution becomes dominant over the exchange of virtual mesons, as found in studies of pion propagation in nuclei [16].

The time-dependent perturbation approach of Ref. [7] relies upon the wave functions of ^{3}He and ^{3}H, which incorporate implicitly the static meson exchange for the NN interaction (the energy dependence of the pion propagator in momentum space, or time dependence in coordinate space, is neglected). Hence, it does not incorporate the energy dependence in the pion exchange, which at the energy which we use is very important [17]. Therefore, the procedure of Ref. [7] is appropriate for low energies, but it becomes less accurate as the energy increases, particularly if one goes beyond the pion production threshold.

In as much as the two-body terms depicted in Fig. 4 are dominated by the exchange of nonstatic pions, as we have argued, there is an easy way to take these processes into account, which is to consider a (γ,π) step (diagram to the left in Fig. 4 if one cuts the intermediate pion line) followed by rescattering of the pion. This is the procedure which we will follow here.

III. TWO-BODY AMPLITUDES IN THE γ ^{3}He$\rightarrow^3$Hπ^+ REACTION

The two most important terms in the $\gamma N\rightarrow\pi^+\pi^-N$ and $\gamma N\rightarrow\pi^+\pi^0N$ amplitudes in the region of interest to us are

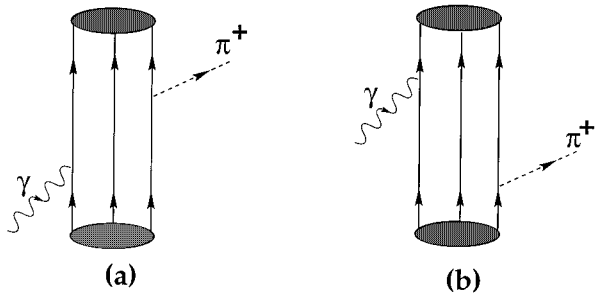

FIG. 3. Two-body mechanism considered in Ref. [7].

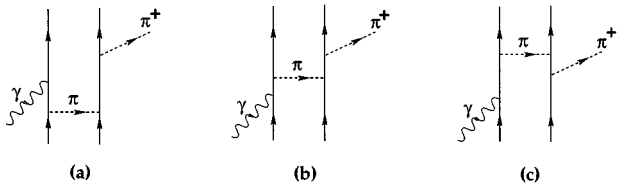

FIG. 4. Feynman diagrams in the time-independent perturbation approach corresponding to the two-body processes of Fig. 3, exhibiting explicitly the exchange of mesons (only π exchange is in the figure).

the Δ–Kroll-Ruderman term and the Δ–pion-pole term depicted in Figs. 5(a) and 5(b), respectively. From there we can construct the two-body meson exchange currents diagrams which would contribute to the (γ,π^+) reaction in ^{3}He. They are depicted in Figs. 6(a) and 6(b), respectively. However, while the diagram of Fig. 6(a) is a genuine two-nucleon exchange currents process, the one in Fig. 6(b) can be classified as a two-body step, $\gamma N\rightarrow\pi N$ in the middle nucleon, followed by the elastic scattering of this pion with the first nucleon. This is of course a possible physical mechanism, but it is automatically taken into account when one considers the (γ,π) process followed by rescattering of the pion, as we shall do. Hence, this term must be excluded from the exchange currents terms in our approach. Thus, we are led to the term of Fig. 6(a) as the dominant MEC term.

By taking the other terms for the $\gamma N\rightarrow\pi\pi N$ amplitude and repeating the former procedure we would get additional terms which generate the MEC in the γ ^{3}He$\rightarrow^3$H π^+ reaction.

There is, however, another term which deserves particular attention. This is the one depicted in Fig. 7(a), which involves Δ excitation followed by $\Delta\rightarrow\Delta\pi$ decay and which gives rise to the exchange currents term of Fig. 7(b) in the γ ^{3}He$\rightarrow^3$H π^+ reaction (DINT, delta interaction mechanism, in the nomenclature of Ref. [18]).

The term in Fig. 7(a) is not particularly relevant in the $\gamma N\rightarrow\pi\pi N$ reaction with on-shell pions since the two Δ's cannot be simultaneously on shell. However, the situation is different in the exchange currents terms of Fig. 7(b) because the pion from the $\Delta\Delta\pi$ vertex is emitted off shell with $q^0=0$ and now both Δ's can be simultaneously on shell, which magnifies the contribution of the term. The pion exchanged in Fig. 7(b) has now a p-wave coupling in both vertices. In such a case it is mandatory to consider simulta-

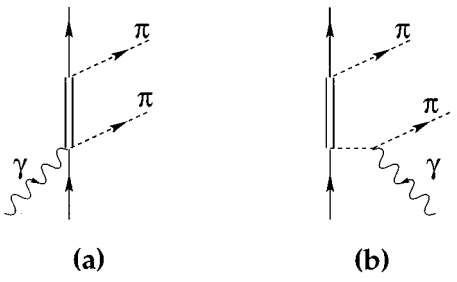

FIG. 5. Dominant Δ–Kroll-Ruderman term (a) and pion pole term (b), in the $(\gamma,\pi\pi)$ process on the nucleon.

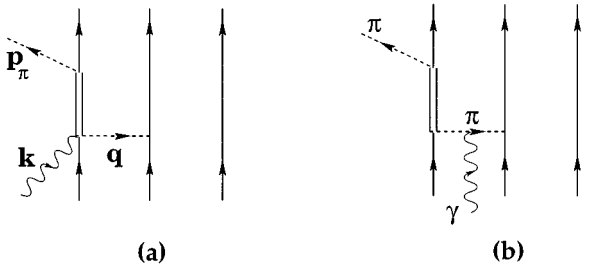

FIG. 6. Meson exchange currents associated to the mechanisms of Fig. 5. Diagram (b) actually corresponds to (γ,π) on one nucleon, followed by pion rescattering on another one, and is treated like that in our approach (see text).

neously the nuclear short-range correlations and supplement it by the exchange of a ρ meson [19] and we do so here.

The differential cross section from the two-body mechanisms of Fig. 6(a) (as well as the other terms generated from the full $\gamma N\to\pi\pi N$ amplitude) is given in the γ ^{3}He c.m. frame by

$$\frac{d\sigma}{d\Omega}=\frac{1}{(4\pi)^2}\frac{M_{\rm He}M_{\rm H}}{s}\frac{p_\pi}{k}|T_{\rm MEC}|^2, \tag{1}$$

with $\vec{k}$ and $\vec{p}_\pi$ the momenta of the photon and the pion, respectively, s the Mandelstam variable for the γ ^{3}He system, and $T_{\rm MEC}$ the two-body scattering matrix given by

$$T_{\rm MEC}=\sum_{l\neq m}\int\frac{d^3q}{(2\pi)^3}F(\vec{q})F(\vec{q}+\vec{p}_\pi-\vec{k}) \times\frac{i}{-\vec{q}^2-m_\pi^2}\frac{f}{m_\pi}\langle\psi_{s,i};^3{\rm H}|t_l\vec{\sigma}_m\cdot\vec{q}\,\tau_m^\lambda|\psi_{s,i};^3{\rm He}\rangle, \tag{2}$$

where $F(\vec{q})$ is the ^{3}He form factor,

$$F(\vec{q})=\int d^3r\varphi^*(r)e^{i\vec{q}\cdot\vec{r}}\varphi(r), \tag{3}$$

with $\varphi(\vec{r})$ the spatial single-particle wave function of the nucleons in ^{3}He or ^{3}H and $\psi_{s,i}$ the spin-isospin wave function. The $\vec{\sigma}$ and $\vec{\tau}$ operators in Eq. (2) refer to the nucleon m while t_l is the $\gamma N\to\pi\pi N$ amplitude referred to the nucleon l.

In a first step we consider harmonic oscillator wave functions corrected by the c.m. motion. This is easily implemented by multiplying by the Tassie-Barker factor the shell model results for the T matrix of Eq. (2), evaluated with the harmonic oscillator wave functions. Hence we have

$$F(\vec{q})F(\vec{q}+\vec{p}_\pi-\vec{k})\to e^{-\vec{q}^2/4\alpha^2}e^{-(\vec{q}+\vec{p}_\pi-\vec{k})^2/4\alpha^2}e^{(\vec{k}-\vec{p}_\pi)^2/12\alpha^2}, \tag{4}$$

with $\alpha^2=0.37$ fm^{-2}. In a second step Faddeev wave functions, which incorporate short-range correlations, will be used.

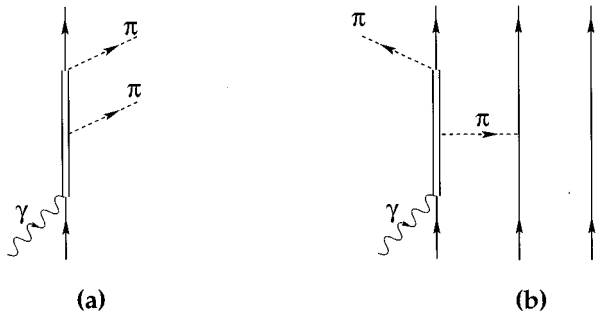

FIG. 7. (a) Successive Δ excitation mechanism for the $(\gamma,\pi\pi)$ process on the nucleon, (b) related meson exchange current mechanism for the (γ,π) reaction on the nucleus (DINT mechanism).

The spin-isospin wave functions for the ^{3}He and ^{3}H can be written by analogy to the quark model wave functions of the nucleons as

$$|\psi_{s,i};^3{\rm He}\uparrow\rangle=\sqrt{\tfrac{1}{6}}(-pnp\downarrow\uparrow\uparrow+npp\uparrow\downarrow\uparrow-ppn\uparrow\downarrow\uparrow +ppn\downarrow\uparrow\uparrow+pnp\uparrow\uparrow\downarrow-npp\uparrow\uparrow\downarrow), \tag{5a}$$

$$|\psi_{s,i};^3{\rm He}\downarrow\rangle=\sqrt{\tfrac{1}{6}}(pnp\uparrow\downarrow\downarrow-ppn\uparrow\downarrow\downarrow-npp\downarrow\uparrow\downarrow+ppn\downarrow\uparrow\downarrow -pnp\downarrow\downarrow\uparrow+npp\downarrow\downarrow\uparrow), \tag{5b}$$

$$|\psi_{s,i};^3{\rm H}\uparrow\rangle=\sqrt{\tfrac{1}{6}}(-pnn\uparrow\downarrow\uparrow+pnn\uparrow\uparrow\downarrow+npn\downarrow\uparrow\uparrow -npn\uparrow\uparrow\downarrow+nnp\uparrow\downarrow\uparrow-nnp\downarrow\uparrow\uparrow), \tag{5c}$$

$$|\psi_{s,i};^3{\rm H}\downarrow\rangle=\sqrt{\tfrac{1}{6}}(-npn\uparrow\downarrow\downarrow+pnn\downarrow\uparrow\downarrow-nnp\downarrow\uparrow\downarrow +nnp\uparrow\downarrow\downarrow+npn\downarrow\downarrow\uparrow-pnn\downarrow\downarrow\uparrow), \tag{5d}$$

where the antisymmetric combination is taken instead of the symmetric one for quarks, for which the color wave function provides the antisymmetry. Given the symmetry of the wave functions, the sum of the two-body operator, $\Sigma_{l\neq m}O_{lm}$, in Eq. (2) can be replaced by $6O_{12}$. Now, in the evaluation of the spin-isospin matrix elements of Eq. (2) with the mechanism of Fig. 6(a) we find, the possible isospin combinations depicted in Fig. 8. We find for the spin-non-flip amplitude,

$$\langle\psi_{s,i};^3{\rm H}|t_1\vec{\sigma}_2\cdot\vec{q}\,\tau_2^\lambda|\psi_{s,i};^3{\rm He}\rangle=A+D, \tag{6}$$

where

$$A=6\langle^3{\rm H}\uparrow|t_1^{(a)}\vec{\sigma}_2\cdot\vec{q}\,\tau_2^\lambda|^3{\rm He}\uparrow\rangle=\sqrt{2}\langle p\uparrow|t^{(a)}|p\uparrow\rangle\langle\downarrow|\vec{\sigma}\cdot\vec{q}|\downarrow\rangle -\sqrt{2}\langle p\uparrow|t^{(a)}|p\downarrow\rangle\langle\downarrow|\vec{\sigma}\cdot\vec{q}|\uparrow\rangle, \tag{7a}$$

$$D=6\langle^3{\rm H}\uparrow|t_1^{(d)}\vec{\sigma}_2\cdot\vec{q}\,\tau_2^\lambda|^3{\rm He}\uparrow\rangle=\sqrt{2}\langle n\uparrow|t^{(d)}|n\uparrow\rangle\langle\downarrow|\vec{\sigma}\cdot\vec{q}|\downarrow\rangle -\sqrt{2}\langle n\downarrow|t^{(d)}|n\uparrow\rangle\langle\uparrow|\vec{\sigma}\cdot\vec{q}|\downarrow\rangle. \tag{7b}$$

On the other hand, for the spin-flip amplitude we find

$$\langle\psi_{s,i};^3{\rm H}|t_1\vec{\sigma}_2\cdot\vec{q}\,\tau_2^\lambda|\psi_{s,i};^3{\rm He}\rangle=A'+D', \tag{8}$$

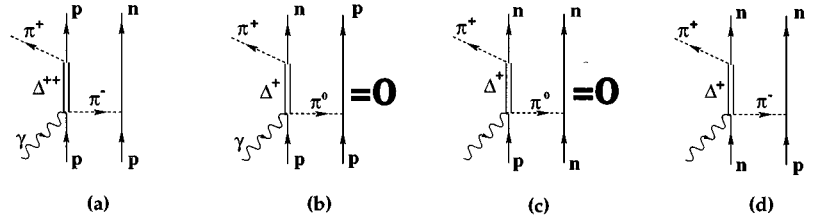

FIG. 8. Detailed diagrams corresponding to Fig. 6(a) which appear in the calculation of MEC's in the $\gamma\ ^3\mathrm{He}\rightarrow{}^3\mathrm{H}\ \pi^+$ reaction.

where

$$A' = 6\langle {}^3\mathrm{H}\downarrow|t_1^{(a)}\vec{\sigma}_2\cdot\vec{q}\,\tau_2^{\lambda}|{}^3\mathrm{He}\uparrow\rangle = \sqrt{2}\langle p\downarrow|t^{(a)}|p\uparrow\rangle\langle\downarrow|\vec{\sigma}\cdot\vec{q}|\downarrow\rangle - \sqrt{2}\langle p\downarrow|t^{(a)}|p\downarrow\rangle\langle\downarrow|\vec{\sigma}\cdot\vec{q}|\uparrow\rangle, \tag{9a}$$

$$D' = 6\langle {}^3\mathrm{H}\downarrow|t_1^{(d)}\vec{\sigma}_2\cdot\vec{q}\,\tau_2^{\lambda}|{}^3\mathrm{He}\uparrow\rangle = \sqrt{2}\langle n\downarrow|t^{(d)}|n\uparrow\rangle\langle\uparrow|\vec{\sigma}\cdot\vec{q}|\uparrow\rangle - \sqrt{2}\langle n\uparrow|t^{(d)}|n\uparrow\rangle\langle\downarrow|\vec{\sigma}\cdot\vec{q}|\uparrow\rangle. \tag{9b}$$

Because of the isospin symmetry, the amplitudes $t^{(a)}$ and $t^{(d)}$ are related by

$$\langle n|t^{(d)}|n\rangle = \tfrac{1}{3}\langle p|t^{(a)}|p\rangle.$$

Thus, the evaluation of the nuclear matrix elements reduces trivially to the spin matrix elements of the elementary $\gamma p\rightarrow\pi^+\pi^- p$ amplitude of Fig. 8(a), removing the nucleon line of the right. This amplitude can be obtained from Ref. [13] and we give it in the Appendix here. Note that the diagrams of Figs. 8(b) and 8(c) are zero in our case.

The unpolarized cross section from the MEC is obtained summing the two cross sections corresponding to the amplitudes of Eqs. (6) and (8). In addition one must consider the photon polarization. This is easily done since

$$t = t^i\epsilon^i(\lambda,\vec{k}), \tag{10}$$

where ϵ^i is the photon polarization in the Coulomb gauge $(\epsilon^0=0,\vec{\epsilon}\cdot\vec{k}=0)$. This allows us also to evaluate the cross sections for polarized photons along the x and y axes and evaluate the asymmetry

$$\Sigma = \frac{\sigma_y-\sigma_x}{\sigma_y+\sigma_x}. \tag{11}$$

On the other hand, the photon unpolarized cross section can be obtained by using

$$\sum_{\lambda}\epsilon^i(\lambda,\vec{k})\epsilon^j(\lambda,\vec{k}) = \delta_{ij} - \frac{k^i k^j}{|\vec{k}|^2}. \tag{12}$$

In addition to the terms in Fig. 8 we would also have a set of terms where the π^+ is produced from the $\gamma N\Delta\pi$ vertex and the exchanged pion comes from the decay of the Δ. In this case this Δ is off shell (has the nucleon energy) and the contribution of these diagrams is much smaller than in the case of Fig. 8. Since close to the Δ pole the Δ propagator in Fig. 8 is purely imaginary $(2/i\Gamma)$, while the terms discussed above are real, there is no interference between the latter terms and those in Fig. 8, and, therefore, their contribution can be neglected. Note that there is one difference between the situation in the MEC and the one met in the $\gamma N\rightarrow\pi\pi N$ with real pions. In this latter case the pion from the $\gamma N\Delta\pi$ vertex in Fig. 8(a) (omitting the nucleon line to the right) has a distribution of energies and so has the Δ. In the case of the exchange currents, the π^- in Fig. 8(a) carries no energy and the Δ can then be placed on shell for a certain energy of the photon. For the same arguments, a term that was important in the $\gamma N\rightarrow\pi\pi N$ reaction, which was the one with $\gamma N\rightarrow N^*(1520)\rightarrow\Delta\pi$, is not so relevant here. The reason is that in $\gamma N\rightarrow\pi\pi N$ with real pions we could have both the $N^*(1520)$ and the Δ close to the on-shell situation since some energy of the $N^*(1520)$ was lost to the pion. However, here the exchanged pion carries no energy and both the $N^*(1520)$ and the Δ will carry the same energy and cannot be simultaneously on shell.

The extension of the formalism discussed in Eqs. (6)–(9) to include the additional terms of the $\gamma N\rightarrow\pi\pi N$ amplitude is easy, since all of them have a structure like in those equations and all one needs is the matrix elements of $t^{(r)}$ between spin-isospin states, which can be obtained from Ref. [14]. We have found that inclusion of these terms changes the contribution of the exchange currents by less than 10% of the contribution of the terms we have discussed, with the only exception being the $\Delta\Delta$ term of Fig. 7 which we pass to discuss below.

The possible terms with the $\Delta\Delta\pi$ interaction are collected in Fig. 9. Note that the structure of the terms (g) and (h) corresponds to the one of diagrams (a) and (d) of Fig. 8, respectively. The contribution of these terms to the nuclear spin isospin matrix element of Eq. (2) is like in Eqs. (7) and

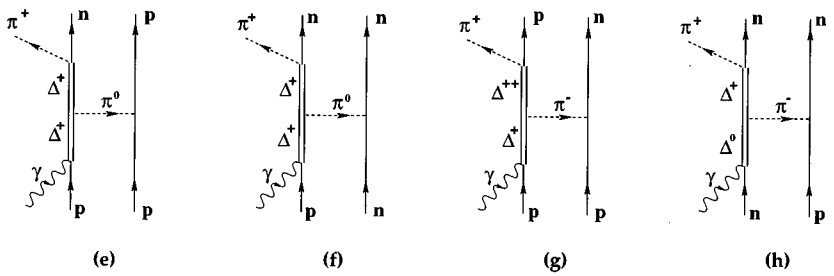

FIG. 9. Detailed diagrams corresponding to Fig. 7(b) which appear in the calculation of MEC's in the $\gamma\ ^3\mathrm{He}\rightarrow{}^3\mathrm{H}\ \pi^+$ reaction.

(9) for the non-spin-flip and spin-flip amplitudes substituting $t^{(a)},t^{(d)}$ by $t^{(g)},t^{(h)}$, respectively. The contribution of the terms (e) and (f) of Fig. 9 is new. We write below the contribution of these diagrams:

$$E=6\langle {}^3\mathrm{H}\uparrow|t_1^{(e)}\vec{\sigma}_2\cdot\vec{q}\,\tau_2^0|{}^3\mathrm{He}\uparrow\rangle=-\langle n\downarrow|t^{(e)}|p\uparrow\rangle\langle\uparrow|\vec{\sigma}\cdot\vec{q}|\downarrow\rangle + \langle n\downarrow|t^{(e)}|p\downarrow\rangle\langle\uparrow|\vec{\sigma}\cdot\vec{q}|\uparrow\rangle, \tag{13a}$$

$$F=6\langle {}^3\mathrm{H}\uparrow|t_1^{(f)}\vec{\sigma}_2\cdot\vec{q}\,\tau_2^0|{}^3\mathrm{He}\uparrow\rangle=\langle n\uparrow|t^{(f)}|p\downarrow\rangle\langle\downarrow|\vec{\sigma}\cdot\vec{q}|\uparrow\rangle - \langle n\downarrow|t^{(f)}|p\downarrow\rangle\langle\uparrow|\vec{\sigma}\cdot\vec{q}|\uparrow\rangle, \tag{13b}$$

and for the spin-flip amplitude we will have

$$E'=6\langle {}^3\mathrm{H}\downarrow|t_1^{(e)}\vec{\sigma}_2\cdot\vec{q}\,\tau_2^0|{}^3\mathrm{He}\uparrow\rangle=-\langle n\downarrow|t^{(e)}|p\uparrow\rangle\langle\downarrow|\vec{\sigma}\cdot\vec{q}|\downarrow\rangle + \langle n\downarrow|t^{(e)}|p\downarrow\rangle\langle\downarrow|\vec{\sigma}\cdot\vec{q}|\uparrow\rangle, \tag{14a}$$

$$F'=6\langle {}^3\mathrm{H}\downarrow|t_1^{(f)}\vec{\sigma}_2\cdot\vec{q}\,\tau_2^0|{}^3\mathrm{He}\uparrow\rangle=\langle n\downarrow|t^{(f)}|p\uparrow\rangle\langle\uparrow|\vec{\sigma}\cdot\vec{q}|\uparrow\rangle - \langle n\uparrow|t^{(f)}|p\uparrow\rangle\langle\downarrow|\vec{\sigma}\cdot\vec{q}|\uparrow\rangle. \tag{14b}$$

From Fig. 9 we can also see that $t^{(e)}=t^{(f)}$. The expression for $t^{(e)}$ can be seen in the Appendix.

An alternative formulation of all these matrix elements, using Racah algebra, is also possible. In the present case, the simple structure of the ^{3}He,^{3}H wave functions allows us this simple direct evaluation of the matrix elements without the use of the elaborate Racah algebra. The calculations have been done with the two methods in order to have extra confidence in the results, which were identical in both cases.

The ρ meson is introduced in an easy way. The amplitudes corresponding to the diagrams in Fig. 9 share in common the structure

$$\hat{q}_i\hat{q}_j D_\pi(q)F_\pi^2(q), \tag{15}$$

where $D_\pi(q)$ is the pion propagator and $F_\pi(q)$ is the πNN form factor. The introduction of the ρ meson is done by replacing this spin-longitudinal combination by

$$(\delta_{ij}-\hat{q}_i\hat{q}_j)D_\rho(q)F_\rho^2(q)C_\rho. \tag{16}$$

From Ref. [20] we have $C_\rho=2.93,\Lambda_\rho=1.4$ obtained from the analysis of the NN interaction, while as shown in Ref. [20], if one takes results from the analysis of $NN\to\pi\pi$ from Ref. [21], this would correspond to $C_\rho=3.94$ assuming the same cut off parameter. We shall see in Sec. V how sensitive the results are to these couplings.

Ordinarily, at the same time that one introduces the ρ meson one introduces the effect of nuclear short-range correlations, which in the absence of the πNN form factors eliminates the δ function implicit in π and ρ exchange. The effects of the short-range correlations modifying the π and ρ exchange are usually included in terms of the phenomenological Landau-Migdal force, of the type $g'\vec{\sigma}\vec{\sigma}\vec{\tau}\vec{\tau}$ [16,19]. In the present case, since we will explicitly use Faddeev wave functions which incorporate the short-range correlations, we shall not introduce this term.

Certainly one can also think about the possibility of exchanging an isoscalar object in Fig. 9, instead of the $T=1$, $\pi+\rho$ exchange. We have estimated the effects of such an exchange and have found it negligible (one order of magnitude smaller at large momentum transfers where the other terms become relevant). The strength of the isoscalar exchange is obtained by imposing that the Δ-Hartree potential in a nucleus is around $-50\rho/\rho_0$ MeV [22]. The momentum dependence of the vertices in the $\pi+\rho$ exchange is what makes the contribution of these terms relatively more important than the isoscalar exchange terms at large momentum transfers.

IV. TOTAL PION PHOTOPRODUCTION AMPLITUDE

In a more elaborated model we shall use realistic three-body wave functions for the ground states of the ^{3}He and ^{3}H nuclei which are obtained as a solution of Faddeev equations with realistic nucleon-nucleon potentials. In the total pion photoproducton amplitude the pion rescattering [or final state interaction (FSI)] will be taken into account.

At present time a large number of three-body wave functions for the $A=3$ system is available. However, most of them give almost the same nuclear form factors in the $0<Q<5$–6 fm^{-1} region. Therefore, we expect that the difference caused by using different sets of Faddeev wave functions is small. In our calculations we will use the wave function obtained in Ref. [23] with the Reid soft-core potential. It describes both static and dynamical properties of the $A=3$ system at momentum transfers up to 6 fm^{-1}, provided one includes meson exchange currents in the electromagnetic observables.

In momentum space the Faddeev wave functions $\Psi(\vec{P},\vec{p})$ are expanded in angular momentum, spin, and isospin bases as

$$\Psi(\vec{P},\vec{p})=\sum_\alpha \phi_\alpha(P,p)|(Ll)\mathcal{L},(S\tfrac{1}{2})\mathcal{S},\tfrac{1}{2}\,M\rangle|(T\tfrac{1}{2})\tfrac{1}{2}\,\nu\rangle, \tag{17}$$

where $\phi_\alpha(P,p)$ are numerical solutions of the Faddeev equations. To shorten the notation we introduced $\alpha=\{Ll\mathcal{L}\mathcal{S}ST\}$, where L, S, and T are the total angular momentum, spin, and isospin of the pair (2,3) (L is associated with momentum $\vec{P}$), and l and $\frac{1}{2}$ have an analogous meaning for the particle (1) (l is associated with momentum $\vec{p}$). The momenta P and p are defined in the Lovelace frame:

$$P=\frac{1}{2}(\vec{p}_2-\vec{p}_3),\quad p=\frac{1}{2\sqrt{3}}(\vec{p}_2+\vec{p}_3)-\frac{1}{\sqrt{3}}\vec{p}_1, \tag{18}$$

where $\vec{p}_1$, $\vec{p}_2$, and $\vec{p}_3$ are the nucleon momenta in an arbitrary frame.

The dominant part of the wave function of Eq. (17) (about 90%) consists of S state components, while the D state probabilities combine to around 8%. It is well known that in the calculation within the impulse approximation the D states give the important contribution in the one-body nuclear form factor at high momentum transfer. However, in the case of MEC's, where two nucleons are involved in the process, we expect that the contribution of the D states will be much smaller since now the momentum transfer is shared between

the two nucleons. Therefore, in calculations of the MEC we shall keep only the biggest S configurations in the expansion of Eq. (17). Then for the nuclear two-body form factor, instead of Eq. (4), we get

$$F(q)F(\vec{q}-\vec{Q})\rightarrow\int d\vec{P}d\vec{p}\,\phi_S(|\vec{P}+\vec{A}|,|\vec{p}+\vec{a}|)\,\phi_S(P,p), \tag{19}$$

where $\vec{A}=\sqrt{3}/2(\vec{q}-\vec{Q}/2)$, $\vec{a}=\vec{Q}/3$, and the transferred momentum $\vec{Q}=\vec{k}-\vec{p}_\pi$.

The total pion photoproduction amplitude, which includes the pion rescattering contributions, can be written as

$$F_{\pi\gamma}(\vec{p}_\pi,\vec{k})=V_{\pi\gamma}(\vec{p}_\pi,\vec{k})-\frac{a}{(2\pi)^2}\times\sum_{\pi'}\int\frac{d^3q'}{M(q')}\frac{F_{\pi\pi'}(\vec{p}_\pi,\vec{q}')V_{\pi'\gamma}(\vec{q}',\vec{k})}{E(p_\pi)-E(q')+i\epsilon}, \tag{20}$$

where the total pion-nuclear energy is denoted by $E(p_\pi)=E_\pi(p_\pi)+E_A(p_\pi)$ and the reduced mass is given by $M(p_\pi)=E_\pi(p_\pi)E_A(p_\pi)/E(p_\pi)$. The factor $a=(A-1)/A=2/3$ is introduced to avoid double counting of the πN interaction in the pion photoproduction $V_{\pi\gamma}$ and pion scattering $F_{\pi'\pi}$ amplitudes.

The nuclear pion photoproduction amplitude $V_{\pi\gamma}$ includes the standard one-body part $V^{\rm IA}_{\pi\gamma}$ obtained using the impulse approximation [1] and the new two-body part $V^{\rm MEC}_{\pi\gamma}$ related to the MEC contributions considered above:

$$V_{\pi\gamma}=V^{\rm IA}_{\pi\gamma}+V^{\rm MEC}_{\pi\gamma}. \tag{21}$$

The amplitude $V^{\rm MEC}_{\pi\gamma}$ is connected with the T matrix in Eq. (2) by the relationship

$$V^{\rm MEC}_{\pi\gamma}=-\frac{1}{4\pi}\left(\frac{M_{\rm He}M_{\rm H}}{s}\right)^{1/2}T_{\rm MEC}. \tag{22}$$

In the framework of the plane wave impulse approximation (PWIA) the one-body part is expressed in terms of the free pion-nucleon photoproduction t matrix:

$$T_{\rm IA}=\langle\pi(\vec{p}_\pi),f|\sum_{j=1}^{A}\hat{t}_{\pi\gamma}(j)|\gamma(\vec{k}),i\rangle, \tag{23}$$

where $|i\rangle$ and $|f\rangle$ denote the nuclear initial and final states, respectively, and j refers to the individual target nucleons. The connection of the $T_{\rm IA}$ matrix with the amplitude $V^{\rm IA}_{\pi\gamma}$ is the same as in Eq. (22). Detailed information about the way of calculating the $V^{\rm IA}_{\pi\gamma}(\vec{p}_\pi,\vec{k})$ amplitude is given in Ref. [1]. For $\hat{t}_{\pi\gamma}$ we shall use the unitary version of the Blomqvist-Laget amplitude [26,27], which describes the real and imaginary parts not only for the resonant magnetic M_{1+} but also for the resonant E_{1+} multipole.

In the formalism which we have used for the construction of the MEC amplitude, the $T_{\rm IA}$ amplitude can be given by

$$T_{\rm IA}=\langle n\downarrow|t_{\pi\gamma}|p\downarrow\rangle e^{-(\vec{k}-\vec{p}_\pi)^2/4\alpha^2}e^{(\vec{k}-\vec{p}_\pi)^2/12\alpha^2} \tag{24}$$

for the case of non spin flip, and by $T'_{\rm IA}$

$$T'_{\rm IA}=-\langle n\downarrow|t_{\pi\gamma}|p\uparrow\rangle e^{-(\vec{k}-\vec{p}_\pi)^2/4\alpha^2}e^{(\vec{k}-\vec{p}_\pi)^2/12\alpha^2} \tag{25}$$

for the case of spin flip.

The pion scattering amplitude $F_{\pi'\pi}$ is constructed in framework of the Kerman-McManus-Thaler (KMT) version of multiple scattering theory [28] as a solution of the Lippmann-Schwinger equation

$$F_{\pi'\pi}(\vec{q}',\vec{p}_\pi)=V_{\pi'\pi}(\vec{q}',\vec{p}_\pi)-\frac{a}{(2\pi)^2}\times\sum_{\pi''}\int\frac{d^3q''}{M(q'')}\frac{V_{\pi'\pi''}(\vec{q}',\vec{q}'')F_{\pi''\pi}(\vec{q}'',\vec{p}_\pi)}{E(p_\pi)-E(q'')+i\epsilon}. \tag{26}$$

Here the pion-nuclear interaction is described by the potential $V_{\pi'\pi}$ which is related to the free πN scattering t matrix [2]. As was shown in Ref. [2] this approach gives a good description of pion-^{3}He elastic scattering in a wide energy region, $50<T_\pi<300$ MeV.

V. RESULTS AND DISCUSSION

In Fig. 10(a) we can see the differential cross section for the two MEC mechanisms discussed in Sec. III. The cross section is calculated at $\theta=137°$ as a function of the photon energy using harmonic oscillator wave functions. The mechanisms peak around the Δ region as expected, and the DINT mechanism involving the $\Delta\Delta\pi$ vertex dominates over the one of the Δ–Kroll-Ruderman term.

In Fig. 10(b) we show the same results but using the Faddeev wave function. We can see that while the Δ–Kroll-Ruderman term contribution barely changes, the one of the DINT mechanism is drastically reduced. This is not surprising in the sense that short-range correlations affect the interaction with two vertices with p-wave coupling, since this interaction contains implicitly the δ term which is suppressed by the correlations. However, the Δ–Kroll-Ruderman term has an s-wave coupling $\vec{S}^\dagger\cdot\vec{\epsilon}$ in one nucleon and a p-wave coupling in the second nucleon, $\vec{\sigma}\cdot\vec{q}$, and the resulting interaction does not contain this short-range piece which is affected by the correlations.

The arguments about correlations can be visualized in Fig. 11, where we plot the relative wave function of two nucleons in ^{3}He using the harmonic oscillator or the Faddeev wave functions. We can see that while the harmonic oscillator wave function has a maximum at zero relative distances, the Faddeev wave function has a hole at small relative distances, as it corresponds to realistic NN forces.

In Fig. 12 we can see the cross sections with the sum of the Δ–Kroll-Ruderman and DINT mechanisms but only π exchange (dashed line) and the contribution of ρ exchange (dash-dotted line). The results are obtained using Faddeev wave functions. We can see that the contribution from ρ exchange is large, as already found in the pion nucleus double charge exchange reaction using the DINT mechanism [18]. We also show in the figure the contribution of the other diagrams for $\gamma N\rightarrow\pi\pi N$, not discussed explicitly before

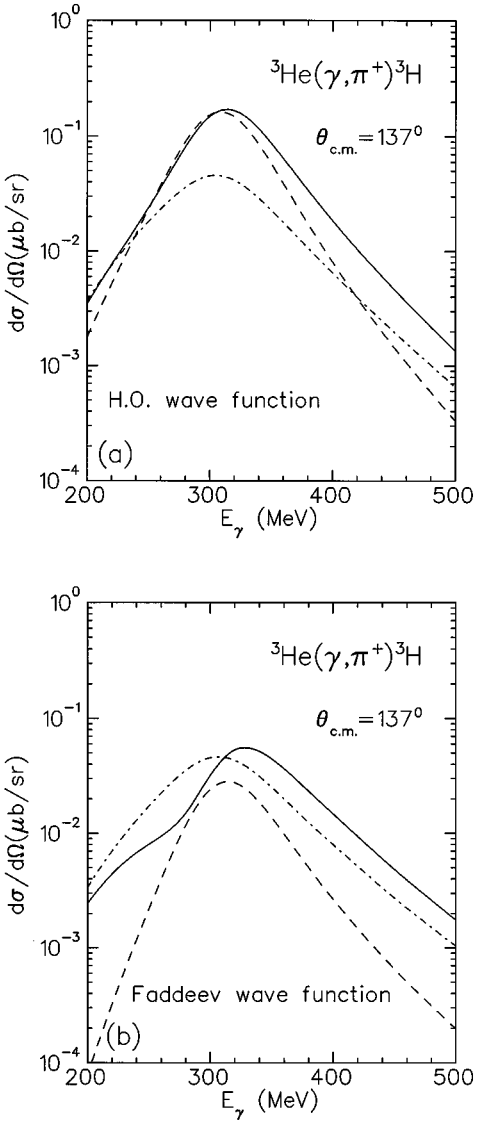

FIG. 10. Energy dependence of the differential cross section at pion angle $\theta_{c.m.}=137°$ for pion exchange DINT (dashed curve) and Δ–Kroll-Ruderman (dash-dotted curve) mechanisms calculated with harmonic oscillator (a) and Faddeev (b) wave functions. The solid curve is the sum of these two MEC mechanisms. The outgoing pion is a plane wave.

(dotted line). As mentioned previously, these terms are small. The results for the sum of all the terms, calculated in the plane wave approximation, are given by the solid line. We also show results using pion rescattering, as discussed in the previous section (thick solid line). The implementation of the pion rescattering reduces the results at photon energies above 250 MeV and moderately increases them at lower energies.

In Fig. 13 we show our results, adding the contribution of the impulse approximation (IA) plus the exchange currents, using pion distorted waves. We can compare the results with the experimental data from Ref. [24]. What we observe is that the MEC contribution (dotted curve) is small at low photon energies and becomes sizable compared to the IA (dashed curve) at high values of Q^2. The MEC's improve the agreement with the data but at large Q^2 we are still short of the experimental numbers.

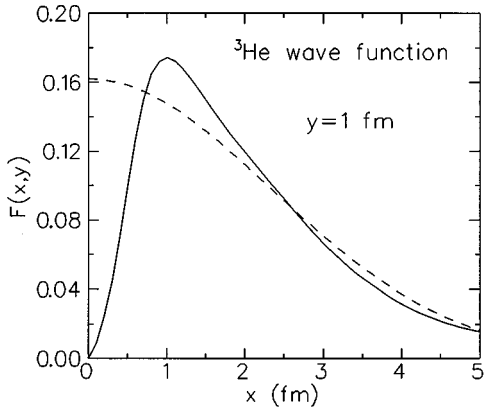

FIG. 11. Harmonic oscillator (dashed curve) and Faddeev (solid curve) wave functions as a function of two-nucleons relative coordinate $x=|\vec{r}_1-\vec{r}_2|$ at fixed $y=|(\vec{r}_2+\vec{r}_3-2\vec{r}_3)/\sqrt{3}|=1$ fm.

Another feature worth noting is that the results are sensitive to the value of C_ρ from Eq. (16) and the $\pi\Delta\Delta$ coupling. If for the latter we take the quark model value $f_\Delta^\pi=\frac{4}{5}f$ [25], where f is the $NN\pi$ coupling constant, $f=1.0$, and take $C_\rho=3.94$ [solid curve labeled (1)], we overshoot the experiment at values of $Q^2=4$–6 fm^{-2}, in a region where the data are fairly reliable. In the same figure we show the results assuming $C_\rho=2.93$, $f_\Delta^\pi=0.8$ (dash-dotted curve) and $C_\rho=2.93$, $f_\Delta^\pi=0.5$ [solid curve labeled (2)]. We can see from all these results that the latter ones, corresponding to the smaller value of C_ρ, together with a similar value of the f_Δ^π coupling as the quark model result, seems to agree better with the data at intermediate values of Q^2. Indications that the $\pi\Delta\Delta$ coupling is indeed smaller than the quark model

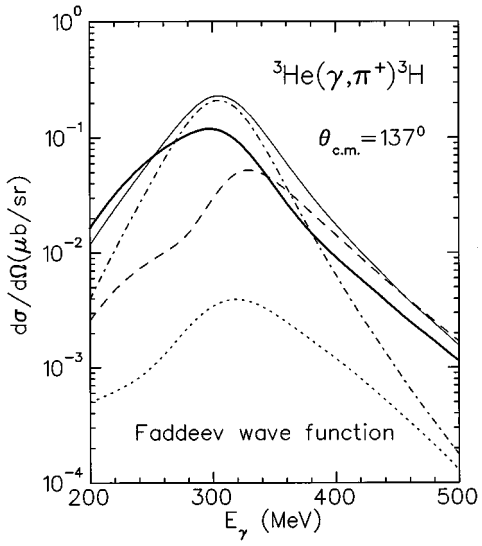

FIG. 12. Energy dependence of the differential cross section at pion angle $\theta_{c.m.}=137°$ for pion exchange DINT + Δ–Kroll-Ruderman (dashed curve), ρ-meson exchange DINT (dash-dotted curve), and others (dotted curve) mechanisms calculated with Faddeev wave functions and plane waves for outgoing pions. The solid and thick solid curves are total MEC cross sections obtained without and with a pion final state interaction, respectively.

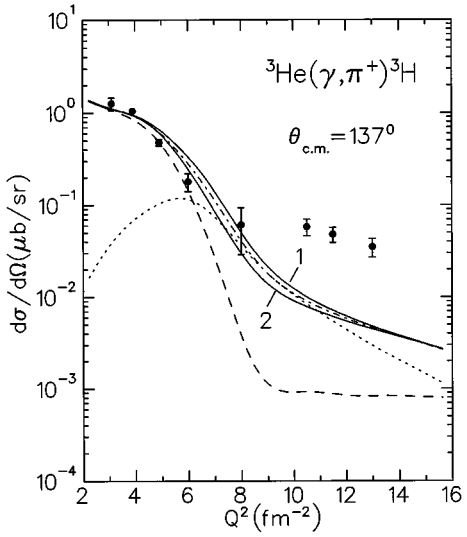

FIG. 13. Differential cross section at $\theta_{\text{c.m.}}=137°$ as a function of the transferred momentum. The dashed curve is the result of the conventional distorted wave impulse approximation (DWIA) approach [1] without MEC contributions. Solid curve (1), MEC's for $C_\rho=3.94$ and $f_\Delta^\pi=0.8$ are included. The corresponding MEC contribution alone is shown by the dotted curve. The dash-dotted and solid curve (2) is the total result for $C_\rho=2.93$ with $f_\Delta^\pi=0.8$ and 0.5, respectively. Experimental data are from Ref. [4].

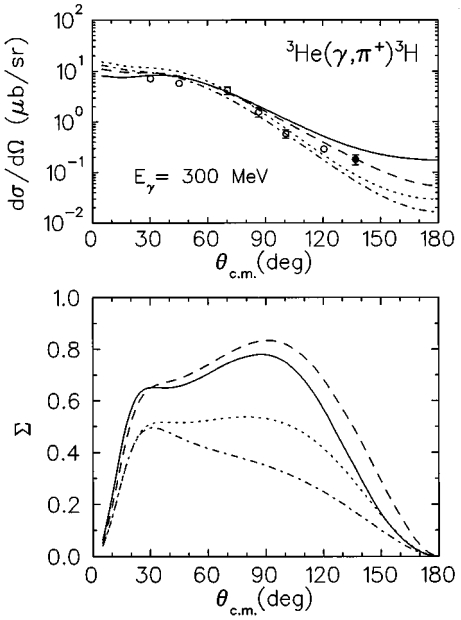

FIG. 14. Angular distribution for differential cross section and photon asymmetry (Σ) at $E_\gamma=300$ MeV calculated with Faddeev wave functions. Dash-dotted and dashed curves are IA and IA +MEC results without FSI's, respectively. Solid curves are the total calculations including FSI's. The dotted curves are PWIA results obtained with harmonic oscillator wave function. In this case the simple relations of Eq. (27) hold. Experimental data are from Ref. [32] (○) and Ref. [4] (●).

result have already been mentioned before in connection with the $\pi N\to\pi\pi N$ reaction [29,30]. Obviously we cannot induce from there the values of f_Δ^π, C_ρ, but we certainly can exclude regions of these couplings where the disagreement with the data would be unacceptable.

Next we would like to discuss the polarization observables. In this paper, we shall consider only single polarization observables that appear in pion photoproduction with a polarized photon and an unpolarized nucleus or an unpolarized photon and a polarized nucleus. In both cases three polarization observables can be measured: the photon asymmetry Σ, target asymmetry T, and recoil asymmetry P.

Definitions and detailed investigations of these polarization observables in the framework of the impulse approximation have been done in Ref. [31]. We recall only one result from this work which will be useful in the discussion below. In a very simple model using harmonic oscillator nuclear wave functions and excluding pion rescattering [the second term in Eq. (20)], we can get simple relations between the observables for ^{3}He$(\gamma,\pi^+)^3$H and the elementary process $p(\gamma,\pi^+)n$:

$$\Sigma(^3\text{He})=\Sigma(p),\quad T(^3\text{He})=-P(p),\quad P(^3\text{He})=-T(p) \tag{27}$$

provided the Lorentz transformation from the πN c.m. to the π ^{3}He c.m. system is taken into account. As was demonstrated in Ref. [31] in the forward direction $\theta_{\text{c.m.}}<60°$ these relations are only slightly destroyed by the complexity of the nuclear structure or by pion rescattering contributions. At larger angles contributions from the nuclear D states and FSI's become important.

In Fig. 14 we demonstrate what can happen with the photon asymmetry when MEC contributions with $C_\rho=2.93$, $f_\Delta^\pi=0.5$ are included in the calculations. There we present the angular distribution for the cross section and the photon asymmetry (Σ) at $E_\gamma=300$ MeV in PWIA (dash-dotted curves), PWIA+MEC (dashed curves), and full calculations with pion rescattering (solid curves). The dotted curves are PWIA calculations with harmonic oscillator wave functions, the model where nuclear polarization observables satisfy the relations of Eq. (27). Thus MEC contributions lead to significant effects in the photon asymmetry and around $\theta=60°-120°$ we can see an increase of the asymmetry by about a factor of 2. We hope that using the recently developed new generation of 100% duty factor high intensity electron accelerators in Mainz, NIKHEF-K(AmPS) and Saskatoon, our prediction for such effects can be verified.

From Fig. 15 we can conclude that target and recoil asymmetries are less sensitive to the MEC contribution at $\theta_{\text{c.m.}}<90°$ (also calculated with $C_\rho=2.93$, $f_\Delta^\pi=0.5$). At backward angles the MEC gives a visible contribution only in the T observable. However, this region (where differential cross sections are small) can also be sensitive to other ingredients of the theory.

VI. CONCLUSIONS

In this paper we have evaluated the contribution of meson exchange currents to the γ ^{3}He$\to^3$H π^+ reaction. For this purpose we used a recently developed model for the $\gamma N\to\pi\pi N$ reaction. The MEC's were evaluated assuming the $\gamma N\to\pi\pi N$ process occurring in one nucleon, producing the outgoing π^+ and one off-shell pion which is absorbed by a second nucleon.

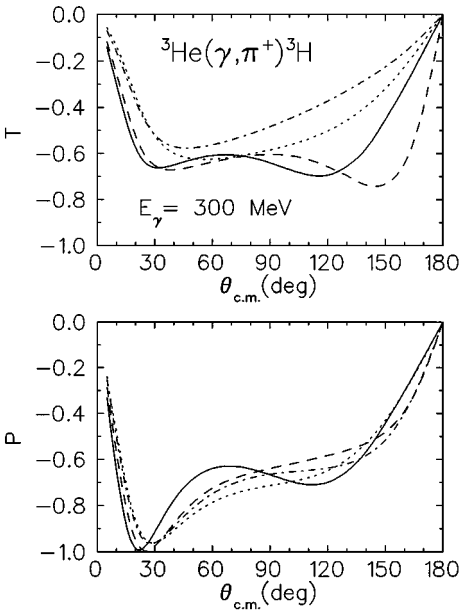

FIG. 15. The same as in Fig. 14 for target (T) and recoil (P) asymmetries.

It was found that, among a large number of Feynman diagrams, those associated with the Δ–Kroll-Ruderman term and the Δ-N interaction were the dominant ones, and the rest were very small. In the latter case of the Δ-N interaction, we also included ρ exchange in addition to pion exchange and it turned out to be important, although quite sensitive to nucleon short-range correlations.

We found the MEC mechanisms to be very important for values of $Q^2=4$–16 fm^{-2}. For values of $Q^2\approx 10$ fm^{-2} we observed an increase of the differential cross section by an order of magnitude with respect to the impulse approximation, improving the agreement with experimental data.

We also evaluated the polarization observables and found that the photon asymmetry was largely affected by the MEC around the Δ resonance region and at angles of about 90^0. A factor of 2 increase in the photon asymmetry was found in this case due to MEC's.

The findings of this paper, both for differential cross sections and polarization observables, and the recent interest in the $\gamma N\to\pi\pi N$ reaction, should stimulate new measurements of the $\gamma\ ^3\mathrm{He}\to{}^3\mathrm{H}\ \pi^+$ reaction with the new improved facilities in order to stress the connection between the elementary $(\gamma,\pi\pi)$ reaction and the (γ,π) reaction in nuclei.

ACKNOWLEDGMENTS

We would like to acknowledge useful discussions with L. Tiator, C. Bennhold, H. Arenhövel, and M. J. Vicente-Vacas. This work is partially supported by CICYT Contract No. AEN-96-1719. One of us (S.S.K.) wants to acknowledge support from the Ministerio de Educacion y Ciencia in his sabbatical stay at the University of Valencia

APPENDIX

In this appendix we show the amplitudes for the Feynman diagrams depicted in Figs. 8 and 9, removing the nucleon line of the right. However, we included here the πNN form factors corresponding to the two vertices in the figure:

$$-it^{(a),(d)}=\mathcal{C}\frac{i}{3}e\left(\frac{f^*}{m_\pi}\right)^2 G_\Delta(p_2+p_\pi)F_\pi((q-k)^2)F_\pi(q^2)\times[2\vec{p}_\pi-i(\vec{\sigma}\times\vec{p}_\pi)]\cdot\vec{\varepsilon}, \tag{A1}$$

$$-it^{(e),(f),(g),(h)}=\mathcal{C}\frac{f^*}{m_\pi}\frac{f_\Delta^\pi}{m_\pi}\frac{f_{\Delta N\gamma}}{m_\pi}G_\Delta(p_2+p_\pi)G_\Delta\times(p_1+k)F_\pi(q^2)\{i\tfrac{5}{6}(\vec{p}_\pi\cdot\vec{k})\vec{q}-i\tfrac{5}{6}(\vec{q}\cdot\vec{k})\vec{p}_\pi-\tfrac{1}{6}(\vec{p}_\pi\cdot\vec{q})(\vec{\sigma}\times\vec{k})-\tfrac{1}{6}(\vec{p}_\pi\cdot\vec{\sigma})(\vec{q}\times\vec{k})+\tfrac{2}{3}(\vec{q}\cdot\vec{\sigma})(\vec{p}_\pi\times\vec{k})\}\cdot\vec{\varepsilon}. \tag{A2}$$

In these expressions, q is the momentum of the π^0 or π^-, p_π is the momentum of the π^+, k is the momentum of the photon, p_1 is the momentum of the incoming nucleon, and p_2 is the momentum of the outgoing nucleon; $G_\Delta(q)$ is the Δ propagator; $F_\pi(q^2)$ is the pion form factor that we take of the monopole type, with $\Lambda=1.3$ GeV; e is the electron charge ($e=0.3027$); f^* is the $\Delta N\pi$ coupling constant, $f^*=2.13$. f_Δ^π is the $\Delta\Delta\pi$ coupling constant. $f_{\Delta N\gamma}$ is the $\Delta N\gamma$ coupling constant, $f_{\Delta N\gamma}=0.116$; $\vec{\epsilon}$ is the photon polarization in the Coulomb gauge ($\epsilon^0=0,\epsilon\cdot\vec{k}=0$).

$\mathcal{C}$ are the isospin coefficients, for each diagram, which are given by

$$\begin{aligned}\mathcal{C}^{(a)}&=1,\\ \mathcal{C}^{(d)}&=1/3,\\ \mathcal{C}^{(e)}&=-\sqrt{2}/6,\\ \mathcal{C}^{(f)}&=-\sqrt{2}/6,\\ \mathcal{C}^{(g)}&=-1,\\ \mathcal{C}^{(h)}&=-2/3.\end{aligned} \tag{A3}$$

[1] S. S. Kamalov, C. Tiator, and C. Bennhold, Few Body Syst. **10**, 143 (1991).

[2] S. S. Kamalov, L. Tiator, and C. Bennhold, Phys. Rev. C **47**, 941 (1993).

[3] R. H. Landau, Phys. Rev. C **15**, 2127 (1977); R. Mach, Nucl. Phys. **A258**, 513 (1976); W. R. Gibbs and B. F. Gibson, Phys. Rev. C **43**, 1012 (1991); M. K. Cheoun, M. Maruyama, S. Ishikawa, and T. Sasakawa, *ibid.* **49**, 1927 (1994).

[4] B. Bellinghausen, H. J. Gassen, E. Reese, T. Reichelt, and P. Stipp, Z. Phys. A **318**, 83 (1984).

[5] S. K. Matthews *et al.*, Phys. Rev. C **51**, 2534 (1995).

[6] A. S. Raskin, E. L. Tomusiak, and J. L. Friar, Few Body Syst. **17**, 71 (1994).

[7] S. S. Kamalov, L. Tiator, and C. Bennhold, Phys. Rev. Lett. **75**, 1288 (1995).

[8] R. C. Carrasco and E. Oset, Nucl. Phys. **A536**, 445 (1992).

[9] J. Ryckebush, M. Vanderhaeghen, L. Machenil, and M. Waroquier, Nucl. Phys. **A568**, 828 (1994).
[10] C. Giusti and F. D. Pacati, Nucl. Phys. **A571**, 694 (1994); S. Boffi *et al.*, *ibid.* **A564**, 473 (1993).
[11] A. Braghieri *et al.*, Phys. Lett. B **363**, 46 (1995).
[12] H. Ströher (private communication).
[13] J. A. Gómez Tejedor and E. Oset, Nucl. Phys. **A571**, 667 (1994).
[14] J. A. Gómez Tejedor and E. Oset, Nucl. Phys. **A600**, 413 (1996).
[15] L. Y. Murphy and J. M. Laget, Report No. DAPHNIA, SPHN 95-42, 1995.
[16] E. Oset, H. Toki, and W. Weise, Phys. Rep. **83**, 281 (1982).
[17] J. A. Gómez Tejedor and E. Oset, Nucl. Phys. **A580**, 577 (1994).
[18] E. Oset, M. J. Vicente Vacas, M. B. Johnson, D. Strottman, H. T. Fortune, and R. Gilman, Nucl. Phys. **A483**, 514 (1988).
[19] G. Baym and G. E. Brown, Nucl. Phys. **A247**, 395 (1975).
[20] R. Machleidt, K. Holinde, and Ch. Elster, Phys. Rep. **149**, 1 (1987).
[21] G. Höhler and E. Pietarinen, Nucl. Phys. **B95**, 210 (1979).
[22] Y. Horikawa, M. Thies, and F. Lenz, Nucl. Phys. **A345**, 386 (1980).
[23] R. A. Brandenburg, Y. E. Kim, and A. Tubis, Phys. Rev. C **12**, 1368 (1975).
[24] D. Bachelier, M. Bernas, J. L. Boyard, J. C. Jourdain, and P. Radvanyi, Phys. Lett. **44B**, 44 (1973); Nucl. Phys. **A251**, 433 (1975).
[25] G. E. Brown and W. Weise, Phys. Rep. C **22**, 279 (1975).
[26] I. Blomqvist and J. M. Laget, Nucl. Phys. **A280**, 405 (1977).
[27] J. M. Laget, Nucl. Phys. **A481**, 765 (1988).
[28] A. K. Kerman, H. McManus, and R. M. Thaler, Ann. Phys. (N.Y.) **8**, 551 (1959).
[29] R. A. Arndt *et al.*, Phys. Rev. D **20**, 652 (1979).
[30] V. Sossi *et al.*, Nucl. Phys. **A548**, 562 (1992).
[31] S. S. Kamalov, L. Tiator, and C. Bennhold, Nucl. Phys. **A547**, 599 (1992).
[32] N. d'Hose *et al.*, Nucl. Phys. **A554**, 679 (1993).